Separation of Ferromagnetic Components by Analyzing the Hysteresis Loops of Remanent Magnetization

**L. R. Kosareva[a], E. V. Utemov[a], D. K. Nurgaliev[a], V. P. Shcherbakov[a, b],
V. E. Kosarev[a], and P. G. Yasonov[a]**

[a] *Kazan Federal University, ul. Kremlyovskaya 18, Kazan, Republic of Tatarstan, 420008 Russia*
e-mail: Lina.kosareva@mail.ru
[b] *Borok Geophysical Observatory, Schmidt Institute of Physics of the Earth, Russian Academy of Sciences,
Borok, 152742 Russia*
Received March 10, 2015

Abstract—The new method is suggested for separating ferromagnetic components in sediments through analyzing the coercivity spectra of the samples by the continuous wavelet transform with the Gaussian-based wavelet (MHAT). A total of 1056 samples of Lake Khuvsgul's sediments (Mongolia) are studied. At least four groups of magnetic components are identified based on the analysis of their magnetization and remagnetization curves. Almost all samples are found to contain two components of bacterial origin which are represented by the assemblages of the interacting single-domain grains and differ by the grain compositions (magnetite and greigite). The applicability of the magnetic data for diagnosing magnetotactic bacteria in sediments and building paleoecological and paleoclimatic reconstructions is demonstrated.

INTRODUCTION

Geological objects typically contain a complex mixture of magnetic minerals of different origin. At present, rock magnetism has separated into an individual research field which offered a variety of methods for exploring the composition, origin, and character of the secondary transformations in the rocks (Sholpo, 1977; Pechersky et al., 2006; Burov et al., 1986; Day et al., 1977; Dunlop and Özdemir, 1997; Evans and Heller, 2003).

A highly interesting and important object for these studies is the bottom sediments of the contemporary lakes, which bear the records of the paleoclimatic (Magny et al., 1993; Thouveny et al., 1994; Peck et al., 1994; Yancheva et al., 2007) and paleomagnetic (Turner et al., 1981; Creer et al., 1983; Thouveny et al., 1990; Ali et al., 1999; Gogorza et al., 2000, etc.) information. Each lake nucleates and evolves in its particular conditions which determine the pattern of its development (Wetzel, 2001; Tundisi and Matsumura-Tundisi, 2011). The integrated effect of the physical, chemical, and biological processes ongoing in a lake specifies the regime of the lake. The results of the interaction between these processes are imprinted in the sediments. A thorough investigation about the properties of the bottom sediments provides valuable information for the changes in the environmental conditions and the events that occurred in the studied territory in the past. An important proxy for environmental changes is the magnetic properties of the sediments containing different magnetic components, e.g., paramagnetic component associated with the grains of clay minerals, as well as allogenic and authigenic components, including the biogenic grains of ferromagnetic minerals. The evolution of the environmental processes can be traced by separately exploring the variations in the properties and concentrations of the magnetic fractions with different origin along a sedimentary column. The possibility for this separation is offered by the analysis of the hysteresis loops of remanent magnetization. V.V. Kochegura (1965) was the first to note the relevance of the information contained in the coercivity spectra of the initial (isothermal) remanent magnetization (IRM). These studies were furthered in (Belokon', 1973; Sholpo, 1977; Thompson, 1986) where the dependences of the coercivity spectra on the grain size and composition of the ferromagnetic fraction were investigated. Considerable progress in quantifying the description of the different phases contained in the sample was made by Robinson and France (1994) who showed that in most cases the IRM curve of the sample which contains a single magnetic fraction is fairly well approximated by the cumulative lognormal (CLG, Cumulative Log-Gaussian) distribution.

Based on this result, Kruiver et al. (2001) and Robertson and France (1994) suggested the method of the statistical analysis of the IRM coercivity spectra (CS) assuming a lognormal distribution for each component and their linear summation in the samples containing a few such components having different parameters. With this approach, each component is fully described by three parameters: the position of the maximum of the spectrum B_{md}, spectral width B_w and the magnetization of a given component M_c. However, it was later demonstrated in (Egli, 2003; Egli, 2004a; Heslop et al., 2006) that this assumption is not valid if there is magnetostatic interaction between the grains, which introduces an asymmetry in the spectral shapes. In this case, the spectral decomposition based on the assumed lognormal distribution will produce additional spectral lines, shift the maxima, and cause other artifacts related to the assumed model.

In order to overcome these difficulties, Egli (2003; 2004a; 2004b) suggested using different model distributions of coercivity which allow for magnetostatic interactions. In his approach, the model functions in the form of generalized lognormal distributions are described by a larger number of parameters. This significantly complicates the problem of spectral decomposition so that even the interpretation of a single spectrum may take a long time.

Taking into account the fact that the selection of the model components (either Gaussian or generalized Gaussian distributions) always sparks a debate concerning the reasonableness of this choice, Heslop and Dillon (2007) designed an alternative approach for analyzing the coercivity spectra which does not require a priori particularizing the ferrimagnetic components. In this method, only the number of the presumed components should be specified, whereas the shape of each individual component is directly found through analyzing the coercivity spectra of a large collection of monotypic samples, assuming that the spectral shape does not change from sample to sample and the only thing that changes is the fraction of the given (each) component.

In 2012, Heslop and Roberts (2012) suggested a new technique for decomposing the hysteresis loop into a few finite terms based on the linear mixing theory. In their method, the end-member compositions do not depend on the types of the curves but instead they are directly derived from the measurements of the hysteresis loops. Particular attention was paid to the shape of the end-members providing the best fit of the expected hysteresis loop of the magnetic minerals.

For completeness, we note that the problem of separating the ferromagnetic components based on a hysteresis loop was also scrutinized in (Stockhausen, 1998; Kruiver et al., 2001; Kruiver and Passier, 2001; Heslop et al., 2002; van Oorschot et al., 2002; Grygar et al., 2003; Spassov et al., 2003; Spassov et al., 2004; Egli, 2004b; Garming et al., 2005). Nevertheless, as seen from the points above, this problem is still a focus

of lively debate concerning both the methods of the analysis and the interpretation of the results. The interest in the problem of isolating the ferromagnetic components is also associated with the necessity to identify the contribution of the biogenic magnetic carriers in the remanent magnetization of the sediments, which is due to the unique properties of the magnetic grains of biogenic origin (the single-domain state and stoichiometry of grains, perfect crystal habit) (Mann et al., 1984; Blakemore and Frankel, 1989; Bazylinski et al., 1994; Heywood åt al., 1990).

In the present paper, by the case study of Lake Khuvsgul's sediments, we propose a new approach to the component analysis of NRM curves from the magnetization and remagnetization data, which applies a continuous wavelet transform with the Gaussian-based wavelet (MHAT).

OBJECT OF STUDY

Khuvsgul is one of the most ancient lakes on the Earth. Its age is more than 5 Ma. The lake's basin is located in north Mongolia (Fig. 1). The basin refers to the western margin of the Baikal Rift Zone. Khuvsgul is the second largest lake of Mongolia. Its area is 5300 km^2, its maximal length if 136 km, and its width is 36 km. The lake is considered to be the deepest water reservoir in Central Asia. Its depth reaches 262 m. The water table of the lake is located 1624 m above sea level.

METHOD

The lake sediments were cored by the drilling complex of PBU Irkutskgeologiya under the joint Russian−Mongolian project. The drill core with a length of 53 m unfortunately has the gaps associated with the core losses due to the different causes. The laboratory testing of the core from the samples taken with an average interval of ~4 cm was carried out at the paleomagnetic laboratory of Kazan State University. For obtaining the spectra of IRM magnetization to 0.5 T, we used the J-meter coercivity spectrometer (Yasonov et al., 2998; Nurgaliev and Yasonov, 2009) capable of separate measurements of the remanent and induced magnetizations of the samples at room temperature. The samples were magnetized from their natural state. Figure 2 shows the example of IRM acquisition curve obtained with J-meter coercivity spectrometer.

MODELING THE COERCIVITY SPECTRA

As shown in the Introduction, a scrupulous approach to describing and identifying the CS requires cumbersome computations, together with fitting a great number of parameters. With this approach, the physical sense of the problem is obscured, and the solution of the problem is reduced to executing a formal, nontransparent procedure. In the present sec-

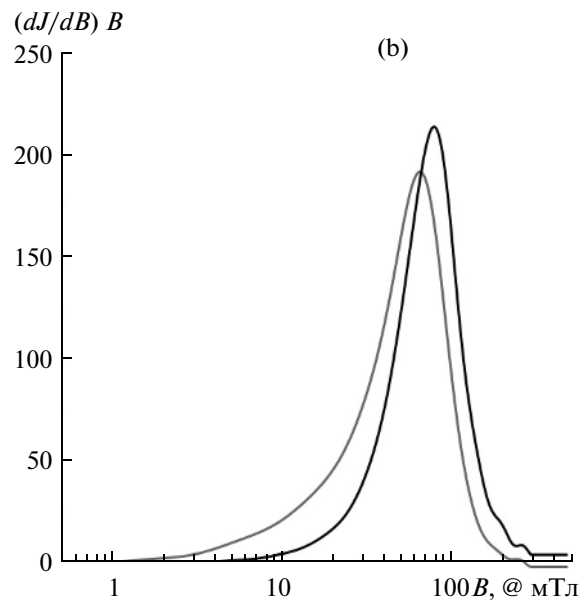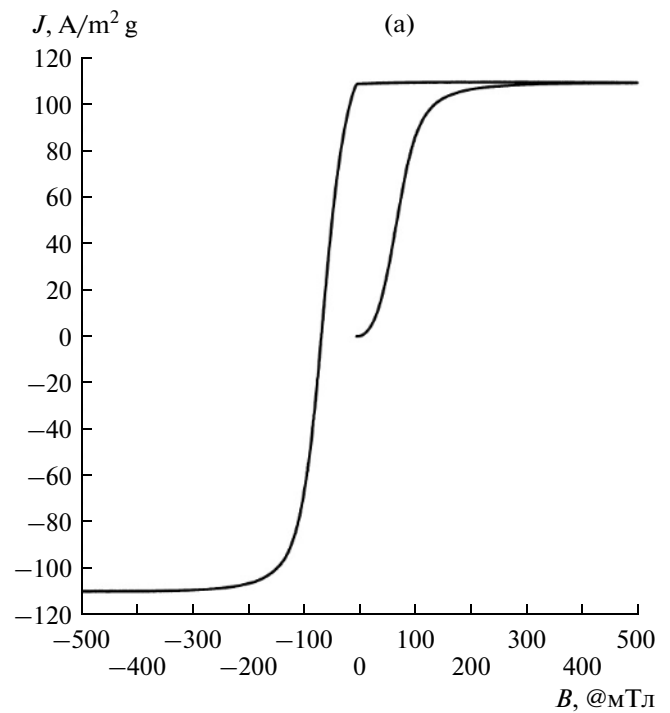Fig. 1. The satellite image of Lake Khuvsgul.

Fig. 2. (a) The remanent magnetization curve; (b) its coercivity spectrum (the black line corresponds to magnetization and the gray line corresponds to remagnetization). Sample c16-166.

tion, we suggest a simple and clear method for visualizing different types of the laboratory IRM based on the simplified treatment of the Preisach–Neel diagram. The advantage of this visualization method is that it enables easy modeling of the magnetization and remagnetization processes of the interacting single-domain (SD) grains and assemblages of multidomain (MD) particles, as well as their different combinations (Belokon', et al., 1973). For simplicity we assume that samples are in a zero state (ZS). In this case, the IRM curve is schematically visualized on the Preisach diagram by filling the OAB area by the elementary hysteresis cycles along the a axis (Fig. 3). When recording the full hysteresis loop, the sample is magnetized up to

saturation as a result of which it acquires the remanent magnetization J_{rs}. After this, the sample is remagnetized in the backfield and, naturally, acquires the remanent magnetization $-J_{rs}$ (Fig. 2). The change in magnetization in the full hysteresis loop corresponds to the double sum of the elementary hysteresis cycles within the OABC rectangle (Fig. 3).

For simplicity, we neglect the vector character of the external field $\mathbf{B}$ and the interaction field $\mathbf{B}_{int}$; i.e.,
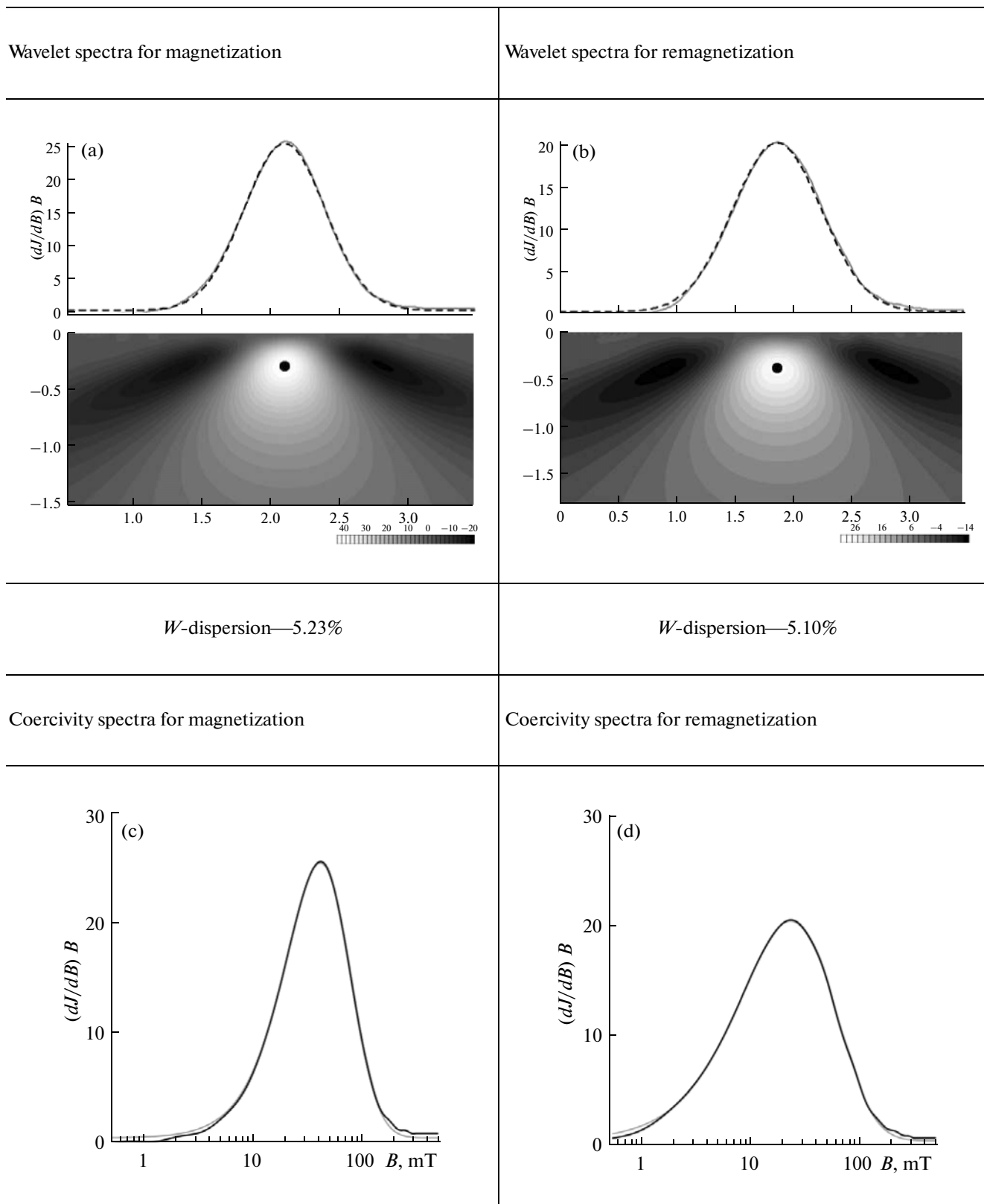
Examples of separating the components of the ferromagnetic fraction in the samples of sediments from Lake Khuvsgul

Sample C11-194

Wavelet spectra for magnetization	Wavelet spectra for remagnetization
W-dispersion—5.23%	W-dispersion—5.10%
Coercivity spectra for magnetization	Coercivity spectra for remagnetization

Table. (Contd.)

Sample C19-94

Wavelet spectra for magnetization	Wavelet spectra for remagnetization
	 W-dispersion—3.87%
W-dispersion—7.17%	*W*-dispersion—3.87%
Coercivity spectra for magnetization	Coercivity spectra for remagnetization

Table. (Contd.)

Sample C21-150

W-dispersion—4.31%

W-dispersion—3.35%

Here, the dashed lines show the CS separation into the main components of the ferromagnetic fraction; the solid black line is the sum of the main components.

we reduce a three-dimensional (3D) problem to a one-dimensional (1D) one. Then, the critical fields a and b can be cast in the following form (Belokon' et al., 1973):

$$a = B_c + B_{int}, \quad b = B_c - B_{int}, \tag{1}$$

where B_{int} is the projection of $\mathbf{B}_{int}$ on the easy axis (axis of easy magnetization) of a grain, and B_c is the critical field of remagnetization of an isolated grain (in the absence of interaction). Since the distribution function (DF) by coercive forces $g(B_c)$ and interaction fields $y(H_{int})$ are independent of each other, we have the following equality for the distribution functions $f(B_c, B_{int}) = g(B_c)y(B_{int})$. On the other hand, from (1) it follows that

$$B_c = (a + b)/2, \quad B_{int}(a - b)/2. \tag{2}$$

For the modeling, we assume a lognormal distribution by coercivity $g(B_c) = (1/Bs\sqrt{2\pi} \times \exp\{-[\ln(B_c/B_{c0})]^2/(2s^2)\}$ and a normal (Gaussian) distribution function by the interaction fields $y(B_c) = 1/(B_m\sqrt{2\pi}) \times \exp[-B_{int}^2/(2B_m^2)]$. Here, B_{c0} is the characteristic coercive force for a given population, s is the root mean square deviation (RMSD) of $\log(B_c/B_{c0})$ from zero, and B_m is the characteristic field of the interaction. This selection is substantiated in (Robertson and France, 1994; Shcherbakov et al., 1991). Then

$$f(a,b) = \frac{1}{2}g\left(\frac{a+b}{2}\right)y\left(\frac{a-b}{2}\right)$$

$$= \frac{1}{4\pi s B_m}\exp\left[\frac{-\ln^2\left(\frac{a+b}{2B_{c0}}\right)}{2s^2}\right]\exp\left(-\frac{(a-b)^2}{4B_m^2}\right). \quad (3)$$

Here, factor 1/2 appears because the Jacobian of the conversion from B_c, B_{int} to a, b is 1/2.

For convenience, in this section we pass to the dimensionless units and measure B_m, VB_{c00}, and B_m in the units of spontaneous saturation magnetization M_s. We recall that $B_{c0} \sim 1$ corresponds to the SD grains and $B_{c0} \approx 0.1-0.3$, to the MD grains. The intensity of the field of interaction between the SD grains is estimated at $5M_sp$ where M_s is spontaneous magnetization and p is the volume density of the grains (Shcherbakov et al., 1991). The characteristic value of p in the sediments is 0.01–0.01; i.e., B_m in the sediments is at most 0.1, which allows us to consider the interaction as weak. However, if the sediment contains biogenic magnetite, the local concentration of the grains can be as high as dozens of percent because the particles are connected into clusters and chains, and in this case the interaction is strong, $B_m \sim 1$. Since in the practical application of our method of magnetic component discrimination we will mainly deal with this case, in the further modeling we will mainly consider the case of a strong interaction.

The examples of the Preisach diagrams calculated by formula (3) are presented in Fig. 4. We note that the diagrams in this figure are located in the upper quadrant in contrast to the traditional scheme where these diagrams are located in the fourth quadrant (Fig. 3).

The shape of the distribution of the density of the elementary hysteresis cycles suggests that this example can be interpreted in terms of a system of the MD grains (Fig. 4a) and strongly interacting SD grains (Fig. 4b). Correspondingly, Fig. 5 illustrates the case when in a sample there is a mixture of strongly interacting SD and MD grains.

The magnetization and remagnetization can easily be calculated if the density of the elementary cycles
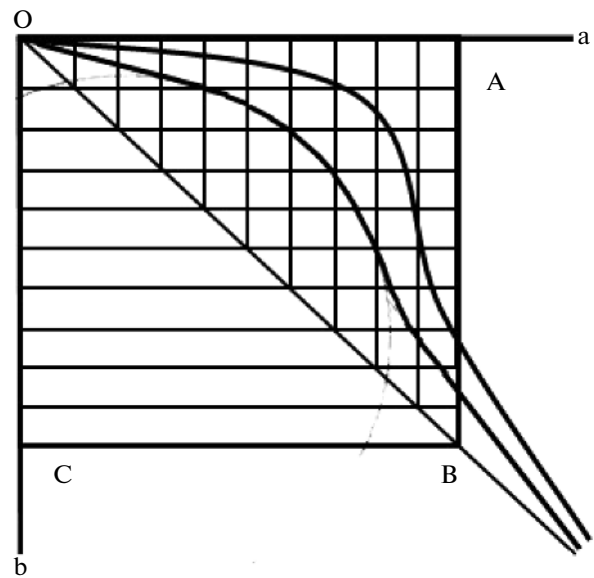

Fig. 3. The schematic of the Preisach diagram. The curved lines schematically show the lines of equal density in the distribution of elementary cycles.

$f(a,b)$ (Belokon' et al., 1973) is known. For the magnetization curve we have

$$J^+(B) = \int_0^B\int_0^a f(a,b)dbda. \quad (4)$$

Here, J is the remanent magnetization of the sample; and the upper index determines the measurement mode (magnetization or remagnetization). The remagnetization curve is

$$J^-(B) = \int_0^\infty\int_0^\infty f(a,b)dadb - 2\int_0^B\int_0^\infty f(a,b)dadb. \quad (5)$$

Differentiation of (1) and (2) gives the following formulas for the coercivity spectra:

$$\frac{dJ^+(B)}{dB} = \int_0^B f(B,b)db; \quad (6)$$

$$\frac{dJ^-(B)}{dB} = 2\int_0^\infty f(a,B)da. \quad (7)$$

When writing out formula (4), we reversed the sign as is commonly done, since any CS is by definition nonnegative. For unifying and comparing the different CSs obtained by formulas (6) and (7), hereinafter we assume them to be normalized by $J^+(\infty)$ and $J^-(\infty)$, respectively.

Figure 5 shows the example of CSA calculated by formulas (6) for the three cases illustrated in Fig. 4. Here, in accordance with the assumed conventions
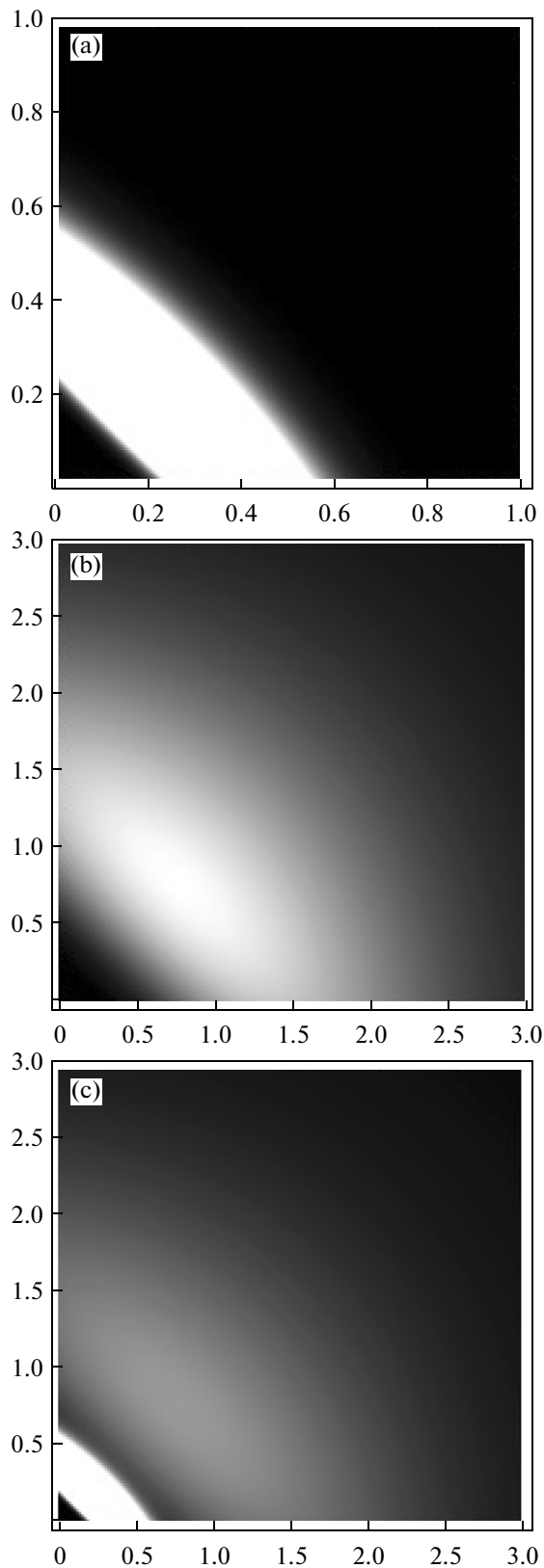
Fig. 5. The coercivity spectra obtained from the isothermal curves of magnetization (the solid line) and remagnetization (the dashed line) for the parameters of DF indicated in Fig. 4: (a) c 0.1; (b) $c = 0.5$. Here, c is the relative contribution of the population of the SD grains in the total remanent magnetization. Correspondingly, the contribution of the MD grains is 1-c.

Fig. 4. The density distribution on the Preisach diagram for (a) $B_{c0} = 0.2$, $s = 0.2$, $B_m = 0.2$; (b) $B_{c0} = 1$, $s = 0.5$, $B_m = 1$; (c) combination of these distributions taken in equal fractions.
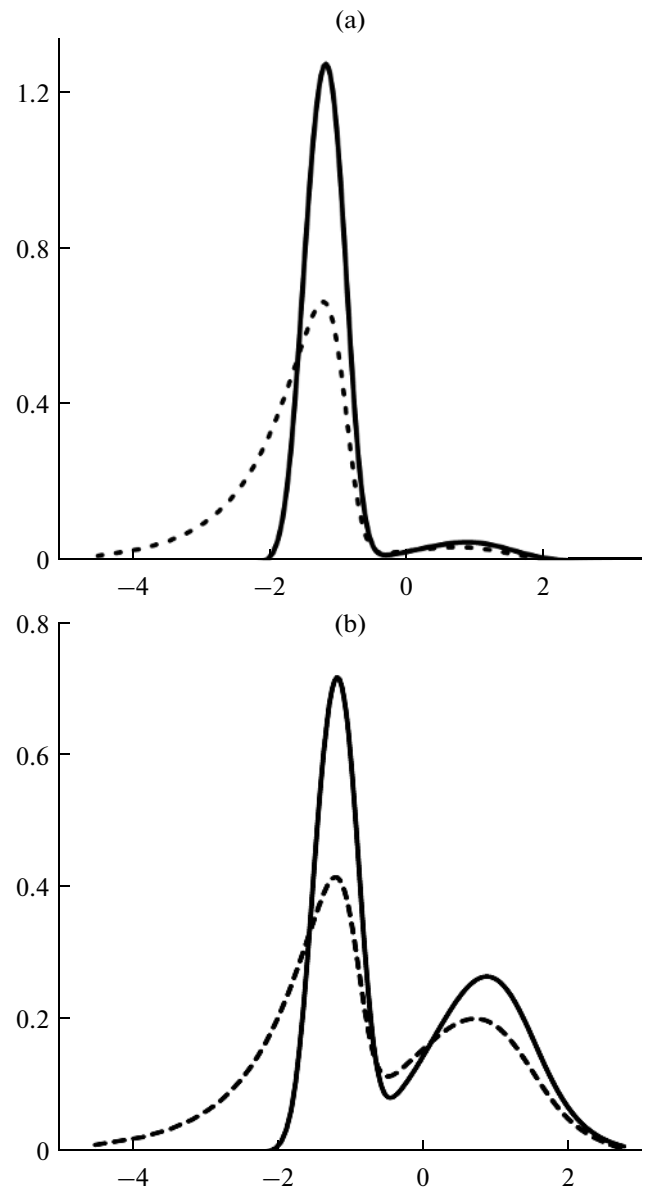
and for easy comparison with the experiment, we passed to the logarithmic derivatives $\dfrac{dJ^+(B)}{dB}B$ and $\dfrac{dJ^-(B)}{dB}B$. Correspondingly, the field along the abscissa axis in this and subsequent figures is also plotted on the log scale. The advantages of this representation of the CS plots were noted in the Introduction.

As seen from Fig. 5, if a sample contains a mixture of the MD and strongly interacting SD grains, these components are easily separated on visual examination if each component introduces at least a 10% contribution to the total value of *J*. Application of the numerical algorithm for separating the CS components and identifying these parameters significantly increases the sensitivity of the suggested method, as demonstrated below.

The experiments show that the coercivity spectrum inferred from the IRM curve is always to a certain extent harder than the spectra for the remagnetization curve (Fig. 2b). The calculations by formulas (6) and (7) support this result (Fig. 6). Besides, let us also consider the fact that the maxima in CS are shifted to the right with the increase in the strength of the interaction. This readily follows from the comparison between Figs. 6a and 6b. Indeed, in the absence of interaction, the maximum in the CS is reached at $B_c = B_{c0}$. Then at $B_{c0} = 0.5$ the peak should be reached at $\log(0.5) = -0.7$, which we see in Fig. 6b where the interaction is very weak. However, in Fig. 6b (in a strong interaction) the CS reaches its maximum at -0.2 to -0.3; i.e., the spectrum becomes visibly harder compared to the real coercivity of the isolated grains. Physically, this is explained by the fact that at the initial ZS the magnetization occurs through the rotation of the magnetic moments of the grains on which the field of interaction $\mathbf{B}_{int}$ is opposite to the magnetizing field $\mathbf{B}$ so that in order to remagnetize the moment of a given particle B should be higher than B_c by B_{int}.

As seen from this figure, the degree of distinction of the coercivity spectra calculated from the initial IRM curve and from the remagnetization curve is proportional to the width of the Preisach diagram along its diagonal, i.e., proportional to the intensity of magnetostatic interaction B_m. In other words, the degree of this distinction can serve as a criterion of the presence of a significant magnetostatic interaction between the grains. The noticeable difference in the spectra can also be associated with the presence of the MD grains, since in this case the density on the Preisach diagram is close to constant within the entire OBCD square (Belokon' et al., 1973). We note that these two cases can be discriminated by the value of the characteristic coercive force B_{c0}. Indeed, for the MD grains we may well expect $B_{c0}/M_s \ll 1$, whereas for the SD grains this ratio should be ~1.

THE CHOICE OF THE BASIS FUNCTION ACCORDING TO THE COERCIVITY SPECTRA OF THE SAMPLES CONTAINING SEINGEL-DOMAIN STRONGLY MAGNETIC FRACTIONS

As a working hypothesis in the analysis of coercivity spectra it is typically assumed that the logarithmic derivatives of these spectra are lognormal (Robertson, France, 1994; Kruiver et al., 2001). In this case, if the external field is taken on the logarithmic scale, the sig-
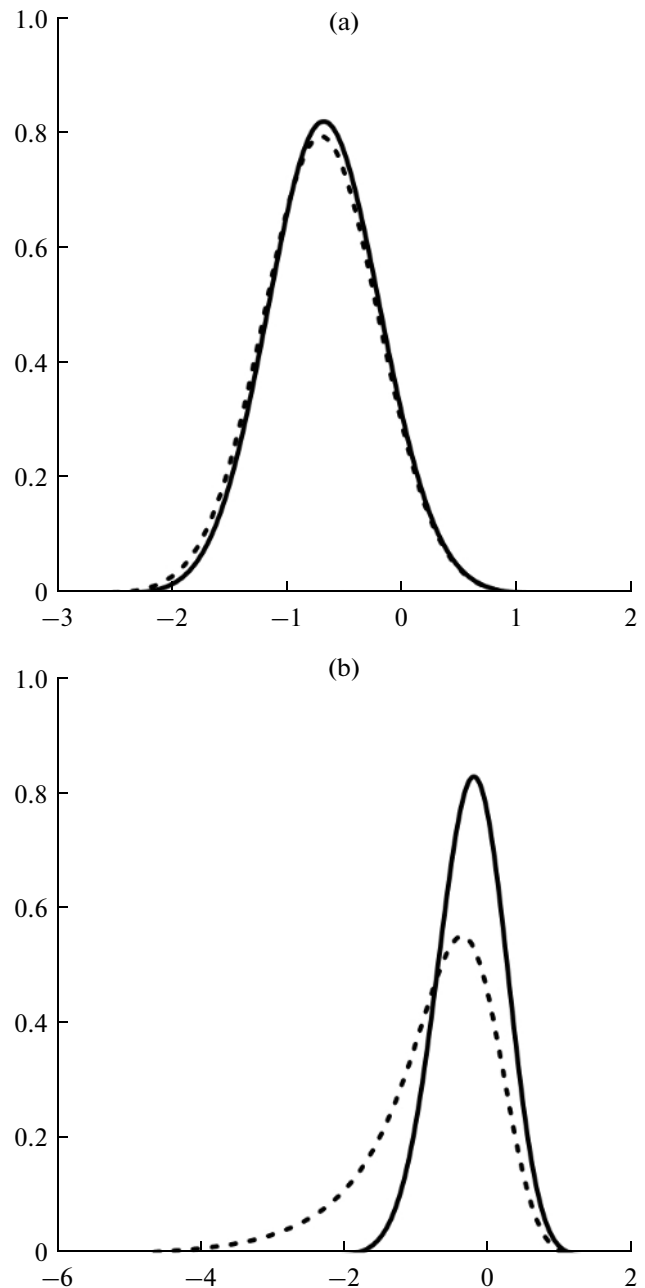

Fig. 6. The coercivity spectra obtained from the curves of isothermal magnetization (the blue line) and remagnetization (the red line) for the parameters of DF (a) $B_{c0} = 0.5$, $s = 0.5$, $B_m = 0.5$; (b) $B_{c0} = 0.5$, $s = 0.5$, $B_m = 0.02$.

nal can be considered as a superposition of the Gaussian curves. In this model, for the sample containing a single magnetic component, disregarding the intergrain magnetostatic interaction, the quantity

$$\frac{dJ}{d(\ln B)} = \frac{dJ}{dB}B \tag{8}$$

on the logarithmic scale should have a shape of a symmetric Gaussian contour.

As seen from formula (3) and Figs. 5 and 6, the presence of the magnetostatic interaction between grains even in the one-component case leads to the violation of the Gaussian form (on the logarithmic scale) of the spectrum and introduces an asymmetry, as was previously noted in (Egli, 2003, 2004; Heslop et al., 2006). In fact, this indicates that the opted model class of lognormal functions is inadequate in the case of significant magnetostatic interaction between grains.

However, the asymmetry in the derivatives of the coercivity curves noticeably diminishes if we pass from the logarithmic to the power-law scale with the numerically fitted value of the power exponent; i.e., if we change the variables. The power-law scale is preferable because the derivative used in this case

$$\sigma \frac{dJ}{dB^\sigma} = B^{1-\sigma} \frac{dJ}{dB} \qquad (9)$$

expands the model class of the lognormal functions. Let us demonstrate this. In the limit $\sigma \to 1$ in (9), we obtain the derivative on the linear scale, and at $\sigma \to 0$ in (8), on the logarithmic scale. Indeed, at small α we have $x^\sigma = \exp[\alpha \ln(x)] \approx 1 + \alpha \ln(x)$, which proves this statement. Hence, parameter α reflects the averaged impact of the forces of the static interaction between the magnetic grains. Clearly, for diminishing the asymmetry of the CS curves, index α was selected in such a way the the modulus of the coefficient of asymmetry was

$$r_1 = \frac{M\left[(X - M[X])^3\right]}{D[X]^{3/2}}. \qquad (10)$$

When processing the data for the coercivity spectra of the studied collection, we used a set of ad hoc samples. It was found that the optimal values of the power index α calculated in the way described are quite stable and lie within $0.2-0.27$.

THE PROCEDURE FOR DECOMPOSING THE COERCIVITY CURVES INTO GAUSSIAN COMPONENTS

The coercivity curves of the magnetization and remagnetization of the samples were averaged by the Chebyshev polynomials of the first kind. The Chebyshev polynomial averaging of the coercivity curves enabled a stable numerical differentiation of the signal on the power-law or logarithmic scale.

In the ideal case, the derivative (9) of the coercivity curve on the corresponding (power-law or logarithmic) scale for multi-component samples is represented by the sum of the Gaussian functions with three unknown parameters: the position of the maximum, the width of the contour, and the amplitude of magnetization of the component:

$$f(x) = \sum_n A_n e^{\frac{(x - m_n)^2}{2y_n^2}}. \qquad (11)$$

The problem of finding the unknown parameters $\{n, A_n, m_n, \sigma_n\}$ in (11) from the measured coercivity spectrum is nonlinear and ill-posed. For solving this problem, we suggest a method based on using a continuous wavelet transform with a "natural" basis (Utemov and Nurgaliev, 2005). The idea of this approach is that the problem of determining the parameters $\{n, A_n, m_n, \sigma_n\}$ can be treated as an inverse problem of finding the parameters of the sources of the Gaussian field by analogy with the inverse problems for potential fields (gravity and magnetic) and their sources. The studied signals are the superposition of the Gaussian functions (11); therefore, the most suitable basis functions for the continuous wavelet transform are clearly those belonging to the family of the derivatives of the same Gaussian function,

$$\psi_m(x) = (-1)^m \frac{\partial^m}{\partial x^m} \exp\left(-x^2/2\right), \qquad (12)$$

since in this case the peculiarities in the shape of the basis function least affect the wavelet spectrum (Astaf'eva, 1996). The optimal choice for family (11) is provided by the second-order wavelet

$$\text{Ш}_2(x) = \left(1 - x^2\right) e^{\frac{-x^2}{2}}, \qquad (13)$$

because with this wavelet the parameters of a single Gaussian source can be determined in the simplest way. Indeed, with the basis wavelet (13) and normalizing coefficient $a^{-1.5}$, the continuous wavelet transform of the Gaussian function with parameters $\{A_0, m_0, \sigma_0\}$ has the following form:

$$W(a, b)$$

$$= A_0 \frac{a y_0}{a^2 + y_0^2} \sqrt{\frac{2pa}{a^2 + y_0^2}} \left(1 - \frac{(b - m_0)^2}{(a^2 + y_0^2)}\right) e^{\frac{(b - m_0)^2}{2(a^2 + y_0^2)}}. \qquad (14)$$

This formula is most easily derived with the use of the Fourier transform and convolution theorem. The central maximum $\{a^*, b^*\}$ of this function is reached at the point with the coordinates

$$a^* = m_0, \quad b^* = \sigma_0, \qquad (15)$$

and has the value

$$W(a^*, b^*) = A_0 \sqrt{\frac{p}{4y_0}}, \qquad (16)$$

i.e., the position and amplitude of the maximum in the wavelet spectrum of the Gaussian field exactly and uniquely determines the position and amplitude of the causative Gaussian source.
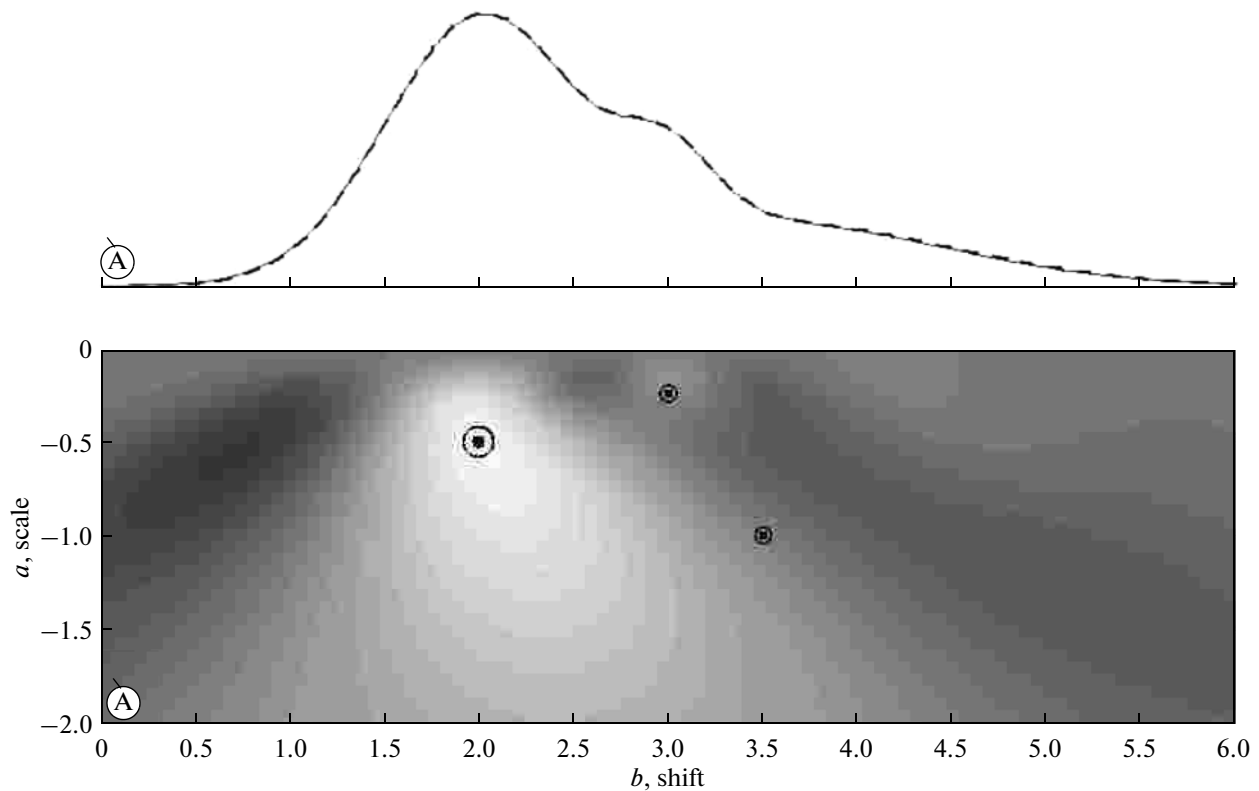
Fig. 7. The example of determining the parameters of the Gaussian sources. (a) The graphs of the given (original) Gaussian field (the thin solid line) and the reconstructed Gaussian field (the heavy dashed line). (b) The centers of the filled circles show the positions of the original sources; the centers of the open circles (rings) mark the positions of the reconstructed Gaussian sources. The background images the wavelet spectra of the original Gaussian field. The sizes of the circles and rings are proportional to the amplitudes of the Gaussian components.

If we deal with interference of the fields from several causative Gaussian sources, formulas (14)−(16) are inapplicable because the extrema of the wavelet spectrum in this case no longer pinpoint the exact location of the sources. A special algorithm has been developed for these situations. To explain this algorithm, we consider the simplest case of interference of two fields from two causative sources. If the parameters of one source are known, then, since the wavelet transform is linear, after subtracting the wavelet spectrum of this source calculated by formula (10) from the total spectrum, the residual values of the wavelet coefficients will describe the spectrum of the second source. Even if we do not know the exact position of the source, the approximate allowance for its parameters will refine the parameters of the second source. By repeating this procedure, we approach the exact solution step-by-step. This principle is also valid for the case of a large number of causative sources. The example in Fig. 7 illustrates the results of reconstructing the parameters of the three given Gaussian sources. As seen from this figure, the parameters are reconstructed quite accurately.

The results of determining the source parameters in a more complex case are shown in Fig. 8. Here, the CS is formed by the MD and SD components with the parameters $B_{c0} = 0.2$, $s = 0.2$, $B_m = 0.2$ (MD component) and $B_{c0} = 1$, $s = 1$, $B_m = 1$ (SD component). The comparison of these parameters with the source parameters obtained by the wavelet method shows that the spectrum becomes visibly harder compared to the actual coercivity of the isolated grains. We note that the parameters of the model are linked with the wavelet-based data through the formulas B_{c0} (shift), $s = \exp$ (scale).

RESULTS AND DISCUSSION

The obtained coercivity spectra of the samples from the sediments of Lake Khuvsgul have a shape characteristic of lacustrine sediments but significantly differ from each other (Fig, 9).

For identifying the components of the ferromagnetic fraction, we carried out the component analysis based on the IRM spectra. The examples of the CS decomposition into components are presented in the table. The parameter W-dispersion shown in Figs. 9a and 9b reflects the degree of closeness of the CS calculated from the obtained sources to the coercivity spectrum measured in the experiment. Quantitatively, this
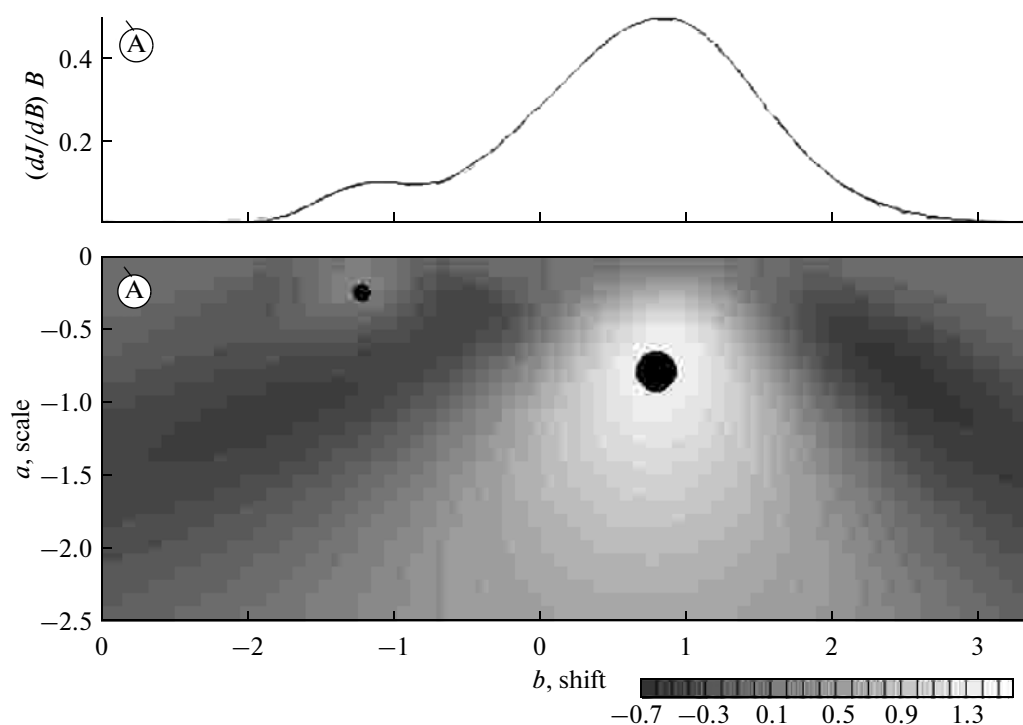
Fig. 8. Left: $c = 0.96$; right: $c = 0.05$. Here, c is the relative fraction of the contribution of the SD component. Top: the coercivity spectra; bottom: the wavelet spectra for the cases indicated above. The parameters of the sources: $B_{c0} = 0.3$, $s = 0.25$ and $B_{c0} = 2.2$, $s = 0.78$.

parameter is a root mean square deviation of the model spectrum from the observed one.

Based on the laboratory studies, Egli (2003) identified a set of the ferrimagnetic components:

(1) EX, extracellular magnetite. This is ultrafine (superparamagnetic) magnetite, a product of iron?metabolising?bacteria. Extracellular magnetite is characteristic of marine and lacustrine sediments, as well as limestones, loesses, paleosoils, and red rocks.

(2) D, detrital magnetite. This component has rather uniform magnetic properties which only depend on the lithology of the drainage basin.

We note that in most cases, the D and EX components overlap in coercivity; therefore, in his works Egli considers them as the total, joining these components into a single D + EX component. The position of the maximum of the coercivity spectrum (PMCS) of this component falls in the interval 0−30 mT. The relatively low hardness of the D and EX components is either due to their high liability to thermal fluctuations (EX) or their pseudo- or multidomain state.

(3) ES, biogenic soft. This relatively magnetically soft component is largely represented by single-domain grains of biogenic magnetic minerals (remnants of magnetotactic bacteria). The exact limits of this component are not reported, approximately indicated as about 40−50 mT, on average 45 mT.

(4) BH, biogenic high. This is a highly coercive biogenic component predominantly including single-

domain grains of magnetic minerals, also biogenic. The exact limits are also not presented, approximately outlined at about 60−90 mT, and on average 73 mT.

According to (Egli, 2003), the PMCS of the bacterial components lie in the interval 30−80 mT, depending on the morphology of the magnetosomes (cubic, prismatic, prolate, or bullet-shaped) and the pattern of their occurrence in cells (isolated, in chains, in clusters, in bundles of chains). Bacterial greigite (BH component) as a rule has PMCS within 75−80 mT (Egli, 2004).

(5) H, high. This component is determined by the presence of highly coercive minerals, e.g., hematite. It is composed of probably allogenic grains, introduced into the sedimentation basin by water flows or by wind.

We have processed the curves of isothermal remanent magnetization and remagnetization for 1056 samples. About 4000 components were identified in these samples. Based on the peaks in the distribution histograms of these components by PMCS (Fig. 10), at least four groups of these components are distinguished.

The first group is clearly detected in the samples of lake sediments by the spectra of isothermal magnetization (Fig. 10a) in the fields of about 5−30 mT. This component fairly well agrees with the data of (Egli, 2003); therefore, following Egli, we also classify this component as D + EX.
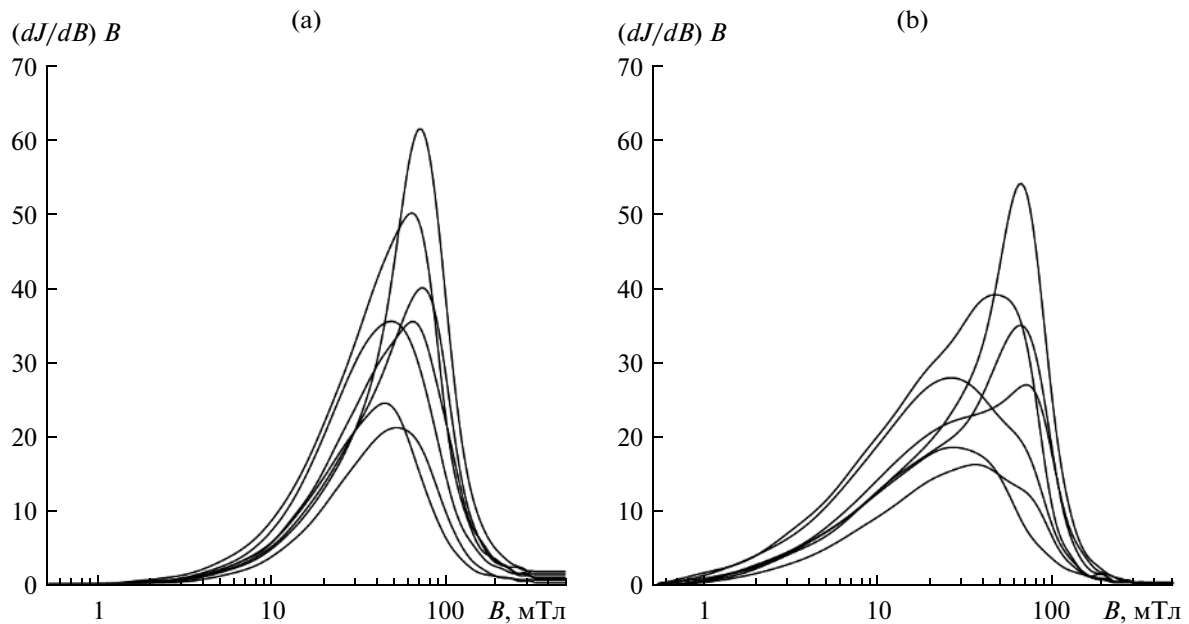
Fig. 9. (a) The coercivity spectra for the magnetization of the samples of the Khuvsgul lake sediments (ñ2-118, ñ6-180, ñ7-126, ñ18k-34, ñ29-206, c31k-106, c32-275); (b) the histogram of PMCS at remagnetization.

Another distinct component is that with PMCS in the magnetization spectra in the interval of ~30−50 mT. In our opinion, this component corresponds to the BS component in the nomenclature of (Egli, 2003).

Next, yet another two peaks are observed in the interval ~50−100 mT. These peaks can probably be identified with the BH component according to (Egli, 2003).

The magnetically hardest component, H, with PMCS at 100 mT and higher is represented by highly coercive grains (hematite, hydroxyls, oxidized magnetite grains, etc.).

The histograms show that the PMCS distributions for the magnetization spectra (Fig. 10a) and remagnetization spectra (Fig. 10b) significantly differ, with the strongest distinctions in the H region. Generally, this difference consists in the increased contribution of the magnetically softer components to the CS obtained from the remagnetization curve. This behavior of the histograms reasonably agrees with the conclusions of the previous sections that the CS determined from the isothermal remanent magnetization curve is always magnetically harder than the one derived from the remagnetization curve. In turn, the difference between these CSs indicates a significant presence of MD grains in the sample in the cases when the soft D + EX component is detected. If this component is absent, the difference of the spectra definitely testifies to the presence of strongly interacting SD grains in the sample, which in the case of sedimentary rocks suggests their biogenic origin.

If we only consider the main ferrimagnetic components of the samples, e.g., by removing all the components which contribute less than 10% to the total remanent magnetization of the samples (Fig. 11), all the peaks described above become more distinct. The BH component (according to (Egli, 2003)) is observed in the interval ~60−85 mT. At the same time, the interval of ~50−65 mT still remains obscure perhaps due to the variability in the grain sizes and shapes of the BS and BH components and the character of the clustering of the grains.

Some of these components are easily identified with the components detected from the spectra of the remagnetization curves (Figs. 10b and 11b). This can be readily done in the cases when these components make up a considerable fraction of the sample's magnetization (Figs. 11a and 11b). However, if we consider all the components including those which contribute less than 10% of the total magnetization of the sample, they are barely identifiable (Fig. 10). The situation is much simpler if we only consider the most significant magnetic components. Here, it is possible to clearly estimate the model values of the PMCS for these components (Fig. 11).

—The D + EX component has the modal PMCS values in the magnetization and remagnetization spectra at ~15−20 and 5−10 mT, respectively. The number of these components in the remagnetization spectra is almost half their number in the spectra of magnetization, which again illustrates the difficulty of identifying the components. Part of the components disappears; these components are probably present in the
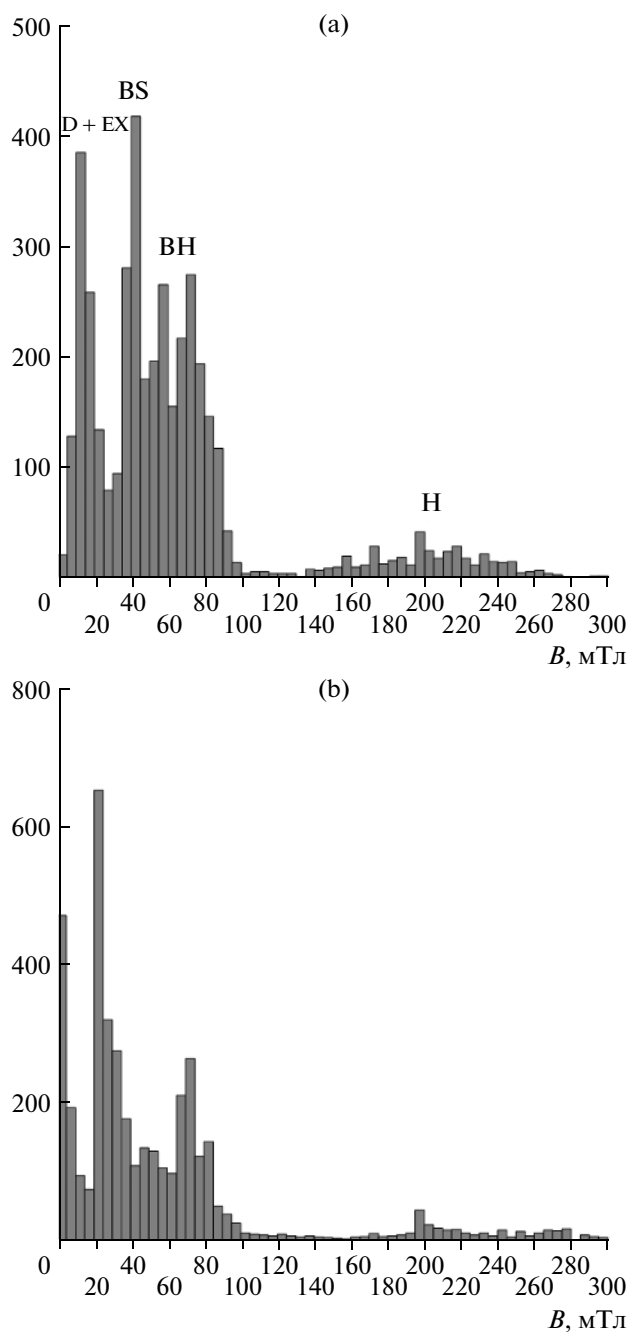
Fig. 10. Identifying the ferrimagnetic components: (a) the distribution histogram of the PMCS of isothermal remanent magnetization; (b) the PMCS histogram for remagnetization.
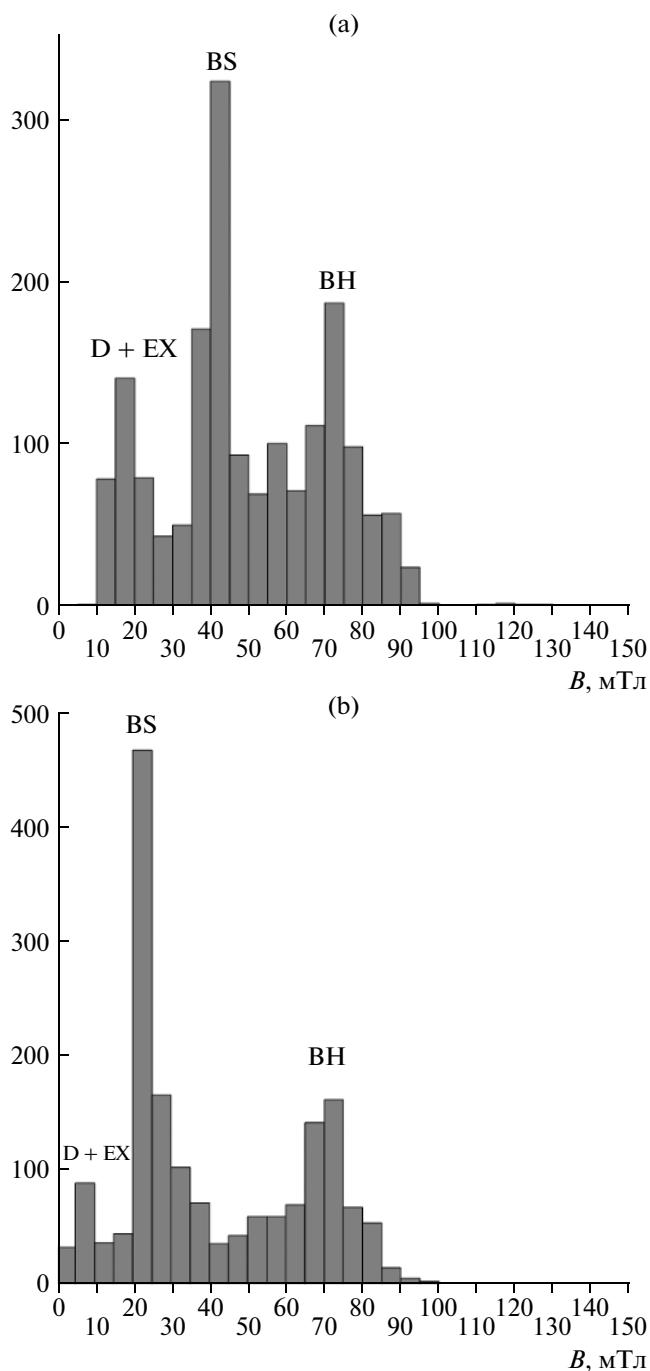

Fig. 11. The histograms of PMCS distribution of the ferrimagnetic components providing more than a 10% contribution to the total magnetization of the sample: (a) identified from the coercivity spectra of the isothermal remanent magnetization; (b) identified from the coercivity spectra of remagnetization.

remagnetization spectra in the form of components having lower magnetization.

—The BS component with the modal PMCS values in the spectra of magnetization and remagnetization in the intervals of ~40–45 and ~20–25 mT, respectively, is distinctly identified. This component is

indicative of the significant interaction fields in this grain assemblage.

—The BH component has very close modal PMCS values in the magnetization and remagnetization spectra, falling in the interval of ~70–75 mT.

—The magnetically hardest H component in all cases accounts for less than 10% of the total magnetization of the samples and is absent in the presented histograms.

We attempted to explore the mineralogical features (Nourgaliev et al., 2005) of the BS and BH components. In order to do this, we conducted thermomagnetic analysis of some samples and collected 18 samples of lake sediments uniformly spaced across the column. Using the Curie express-balance (Burov et al., 1986), we measured the temperature dependence of induced magnetization at a heating rate of 10°C per minute up to 700°C. For estimating the contributions from the components with different magnetic hardnesses, the curves were measured at two intensities of the magnetic field (0.05 and 0.2 T). The curves of the first and second heating enabled us to estimate the mineralogical transformations in a sample. The second curve was measured on the same sample after its cooling to room temperature. The thermomagnetic data were compared with the results of the decomposition of the coercivity spectra. Based on this analysis, all the samples were classified into two main groups.

Group 1. The magnetization of the sample is dominated by the contribution of the BS component. This group comprises four samples. The example in Fig. 12 shows the comparison of the TMA data and the decomposition of the coercivity spectra for sample c10-36. In fact, there is only one magnetic component in this sample. The thermomagnetic curve also shows the presence of a single magnetic phase (magnetite). Significant mineral transformations do not occur during the first heating (the magnetization of the sample after the first heating remains unchanged) except for the fact that the grains after the first heating become magnetically harder. This follows from a certain difference between the curves of the first and second heating obtained in a lower field (0.05 T) (Fig. 12a). The thermomagnetic curves in the stronger field almost coincide (Fig. 12b). Perhaps we are dealing here with highly pure magnetite, not oxidized, and almost without signs of maghemite.

Group 2 incorporates all the remaining samples. The examples of two extreme cases from this group are illustrated in Figs. 13 and 14. Several components are revealed in all samples according to the results of the decomposition of the coercivity spectra. Among these, the BS and BH components are reliably identified, BS being predominant in all cases. In sample c24-6 (Fig. 13) the percentage of the BH component is somewhat higher than in sample c11-11- (Fig. 14). The thermomagnetic curves of these samples drastically differ from the curves obtained for the samples only containing the BS component (Fig. 12). Firstly, during the first heating the magnetization grows due to the magnetite formation resulting from the dissociation of iron sulfide. This is indicated by the peak in the differential TMA curve in the area of 450−500°C (Burov et al., 1986). The increase in magnetization

after the first heating in sample c11-110 is significantly higher than in sample c24-6; however, the peak in the interval of 450−500°C in this sample is less distinct. Perhaps this is due to the fact that magnetite formed in sample c11-110 has a very small size and the blocking temperature of the grains is far below 450°C. In sample c24-6, iron sulfide is likely to have larger grains. Among the detected iron sulfides there could also be greigite, as suggested by the presence of a small peak between 250 and 300°C in the thermomagnetic curves, characteristic of the thermomagnetic behavior of this mineral (Burov et al., 1986).

Now a few words about some effects revealed in the presented thermomagnetic curves.

—The peak detected in the differential TMA curves in the interval of 150−200°C (Figs. 12, 13, and 14) is due to the change in the magnetic hardness of the oxidized magnetite (BNurov et al., 1986).

—The differential TMA curves of the second heating for the samples containing sulfides fix the magnetic phase above 600°C; this is greigite. Considering the fact that it was produced through the oxidation of magnetite resulting from iron sulfide, the formation of a significant amount of very fine grained magnetite which has been immediately oxidized to hematite is probable.

DISCUSSION

Unfortunately, we have not been able yet to take the electron microscopy images of the magnetic separates from the studied samples. However, even now it can be stated that the revealed BS and BH components are highly probably biogenic. This is suggested by the PMCS distributions containing a few distinct components which are stably tracked throughout the studied history of the basin. It is barely conceivable that an occasional process of weathering and sedimentation could produce the observed assemblages of the magnetic grains whose properties would have been preserved throughout a few hundred thousand years against significantly varying ambient conditions (Fedotov et al., 2004). Among these components there are two which are very similar to those identified by Egli (2004). Therefore, by analogy, we termed these components BS and BH. The weak average field of intergrain interaction is characteristic of these components, as follows from the rather small shift between the PMCS of the magnetization and remagnetization spectra. This also testifies to the single domain grain assemblage and its biogenic origin.

Thus, with the suggested methods it is possible to obtain the express data about the remains of magnetotactic bacteria in sediments. Moreover, this approach even enables the separation of these components without their segregation and direct observations. In fact, this is a new method for paleontology studies. The first question arising on this is how the BS and BH components differ. There can be a variety of sources of their
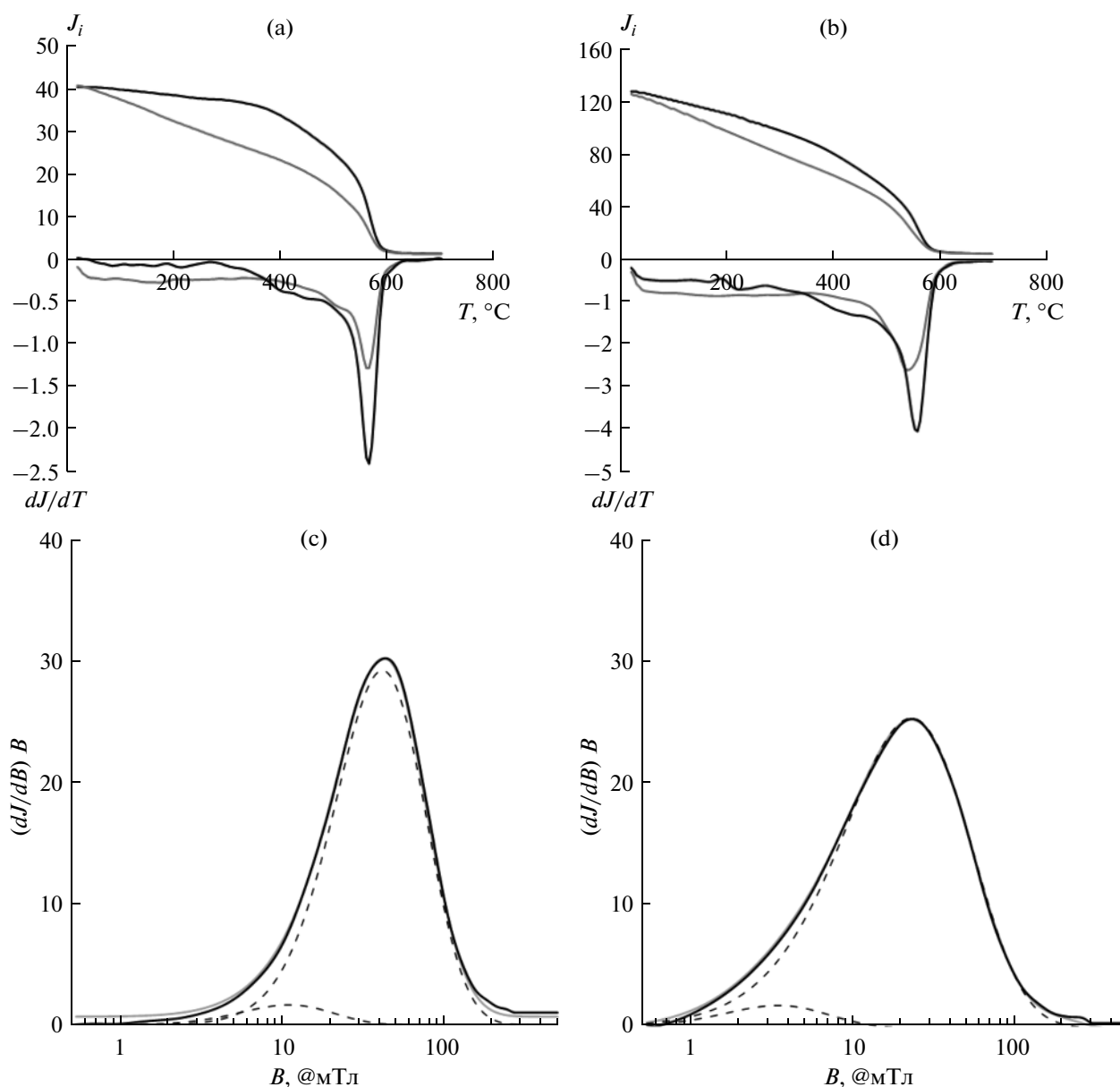
Fig. 12. The example of comparing the TMA data with the decomposition of coercivity spectra. Sample c10-36. Top line: the TMA diagrams; the black line shows the first heating; the gray line shows the second heating. The top and the bottom parts of the diagram is the integral and the differential curves, respectively; (a) in the field of 0.05 T; (b) in the field of 0.2 T. The bottom line: the coercivity spectra for (c) magnetization and (d) remagnetization. The gray line is the averaged coercive curve; the dashed lines show the separation of the coercivity spectrum into the main components; the solid black line corresponds to the sum of the main components.

difference, including the shapes and sizes of the grains and mineralogy. All these parameters clearly have a paleontological value. In our case, we attempted to find out whether the difference between the BS and BH components is due to their mineral composition. The obtained thermomagnetic data evidently show that the BS component is represented by the assemblage of magnetite grains. The arguments proving this fact are shown in Fig. 13. Moreover, it can be stated quite positively that magnetite in these samples does not contain maghemite and is sufficiently pure. This

also follows from the fact that the thermomagnetic effect in the interval 150–200°C, which is typically associated with magnetite from the hypergenesis zone, is very weak. We note that these samples do not contain other strong magnetic minerals (e.g., sulfides). However, as soon as the signs of the BH component appear in the decompositions of the coercivity spectra, the thermomagnetic curves immediately come to have the signs of the presence of iron sulfides in the samples. One of the sulfides is greigite whose presence is detected by the thermomagnetic effect in the interval
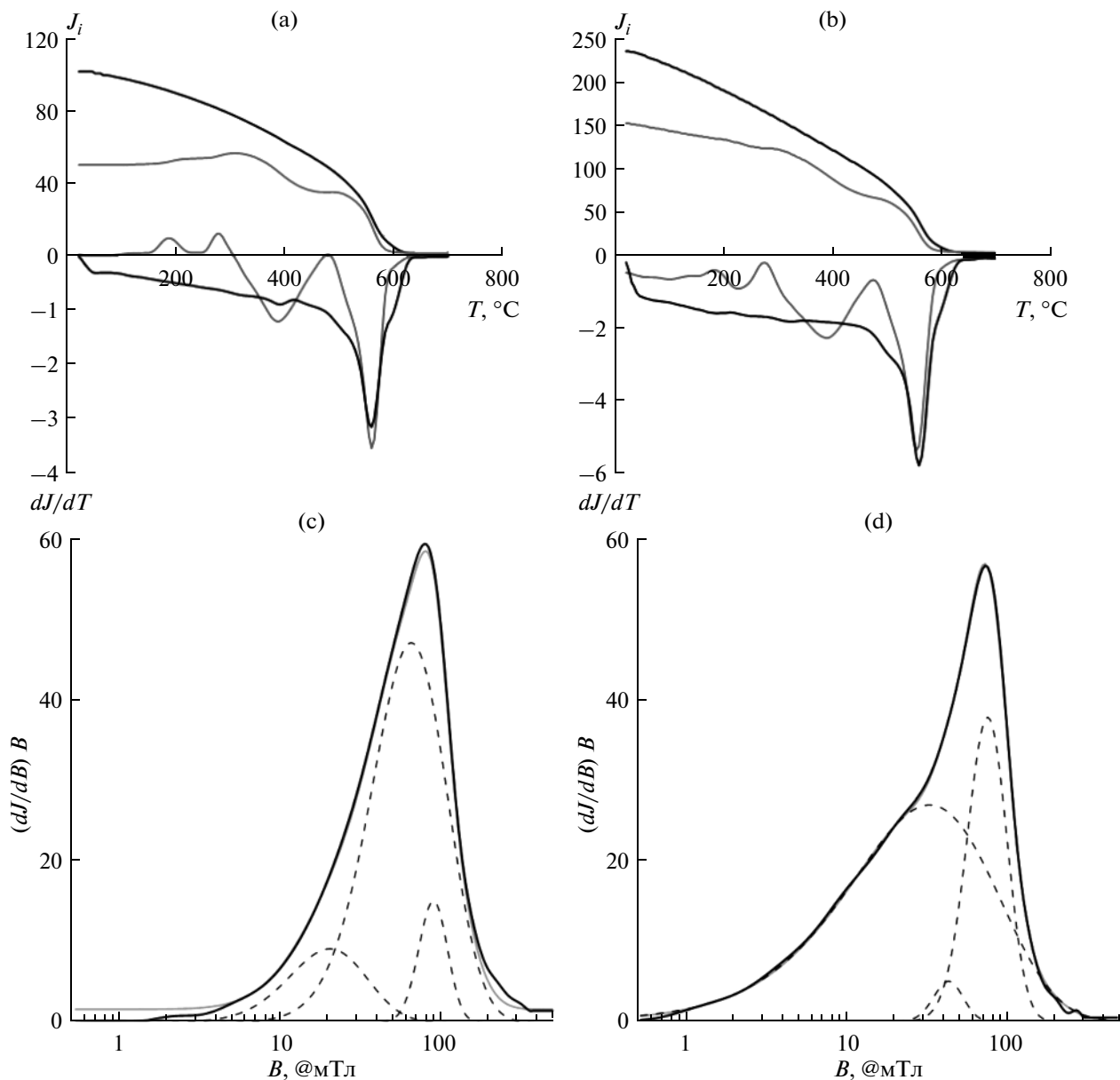
Fig. 13. The example of comparing the TMA data with the decomposition of coercivity spectra. Sample c24-6. Top line: the TMA diagrams; the black line shows the first heating; the gray line shows the second heating. The top and the bottom parts of the diagram are the integral and the differential curves, respectively; (a) in the field of 0.05 T; (b) in the field of 0.2 T. The bottom line: the coercivity spectra for (c) magnetization and (d) remagnetization. The gray line is the averaged coercive curve; the dashed lines show the separation of the coercivity spectrum into the main components; the solid black line corresponds to the sum of the main components.

$250-300°C$. Thus, we may attribute the difference between the BS and BH components to the mineralogical factors. It is also worth noting that we have not yet found the samples which would only contain the BH component alone. This component always cooccurs with the BS one. This fact is very interesting. It can be associated with either the redeposition of the grains composing the BS component, or the probable simultaneous generation of the both components. The second hypothesis appears fascinating. In our opinion, there could be two boundaries within the water layer

where magnetotactic bacteria may dwell. In this case, the changes in the ratio between the abundances of different types of magnetotactic bacteria result from the changes in the water balance in the basin due to the climatic and tectonic impacts. Thus, the remanent magnetization and hysteresis parameters acquire a new quantitative paleoecological sense: they provide the basis for estimating the amount of the remains of different types of magnetotactic bacteria per unit sediment volume, as well as their mineralogical and morphological characteristics. This express information
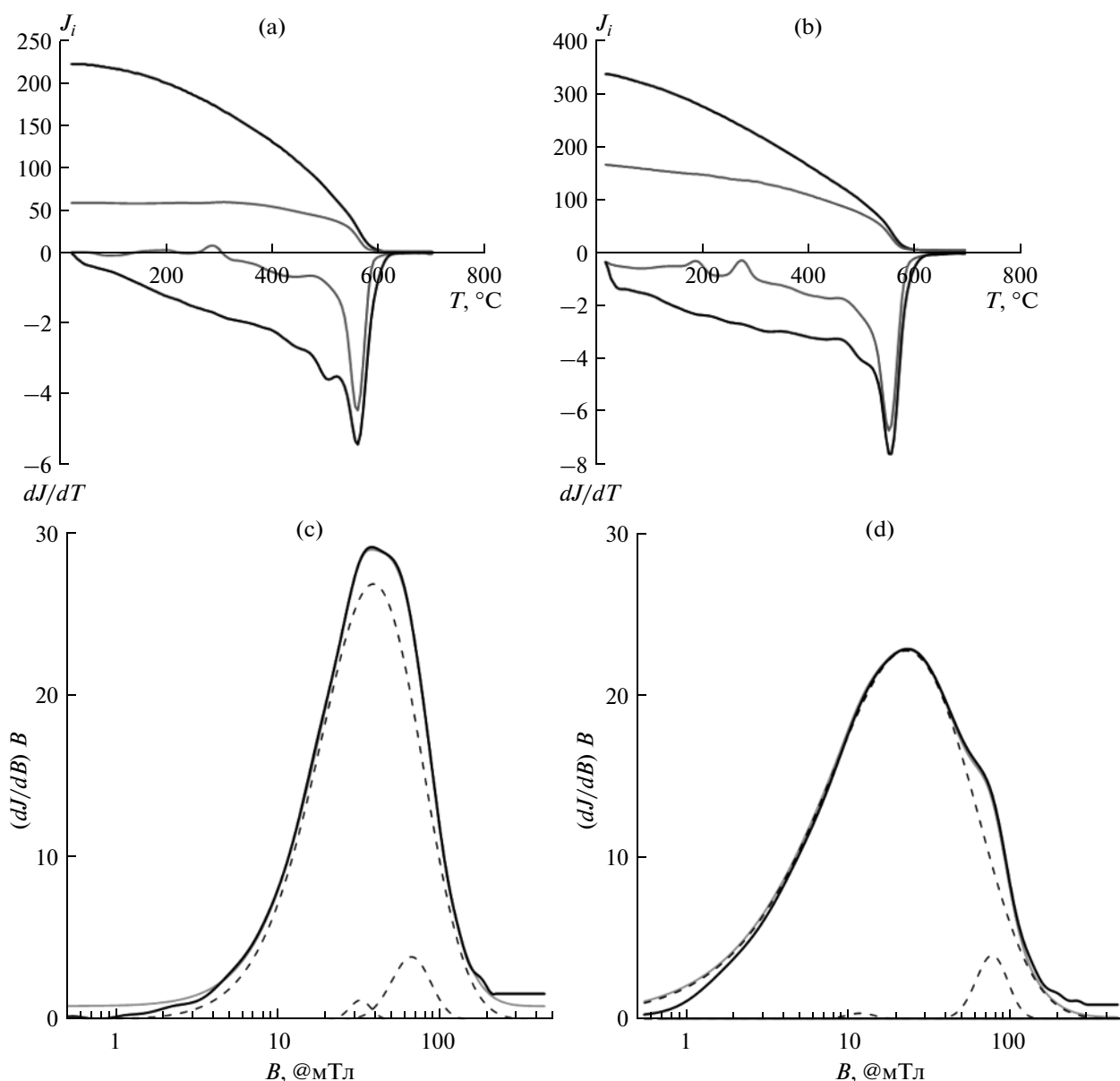
Fig. 14. The example of comparing the TMA data with the decomposition of coercivity spectra. Sample c11-110. Top line: the TMA diagrams; the black line shows the first heating; the gray line shows the second heating. The top and the bottom parts of the diagram is the integral and the differential curves, respectively; (a) in the field of 0.05 T; (b) in the field of 0.2 T. The bottom line: the coercivity spectra for (c) magnetization and (d) remagnetization. The gray line is the averaged coercive curve; the dashed lines show the separation of the coercivity spectrum into the main components; the solid black line corresponds to the sum of the main components.

about the presence of different types of magnetotactic bacteria and their ratio in the sediments open up new fields of use of rock magnetism for obtaining paleoreconstructions of the environment and paleoclimate based on the data on lake sediments.

CONCLUSIONS

The wavelet decomposition of the coercivity spectra into Gaussian components is a suitable instrument for identifying the magnetic assemblages of different origin in the sediments of contemporary lakes. The express character of deriving these data (measurement of the curves with the use of the coercive spectrometer and decomposition of the coercivity spectra) enables us to process the extensive collections of samples. This offers new possibilities for applying the methods of rock magnetism in the paleoecological and paleoclimatic studies.

Based on the coercivity spectra of the samples from Lake Khuvsgul, several magnetic components are revealed, among which there are two biogenic compo- ₃ nents with different magnetic hardness, identified by a

2 number of signs. Based on the data of the thermomagnetic analysis it is established that the soft component is represented by magnetite grains and the hard com-
1 ponent, by greigite. These data can be used for reconstructing the changes in the environment and climate variations from lake sediments.

REFERENCES

Astaf'eva, N.M., Wavelet analysis: basic theory and some applications, *Physics—Usp.*, 1996, vol. 39, no. 11, pp. 1085–1108.

Bazylinski, D.A., Garratt-Reed, A.J., and Frankel, R.B., Electron microscopic studies of magnetosomes in magnetotactic bacteria, *Microsc. Res. Tech.*, 1994, no. 27, pp. 389–401.

Belokon', V.I., Kochegura, V.V., and Sholpo, L.E., *Metody paleomagnitnykh issledovanii gornykh porod* (Methods of Paleomagnetic Studies of Rocks), Leningrad: Nedra, 1973.

Blakemore, R.P. and Frankel, R.B., Biomineralization by magnetogenic bacteria, in *Metal-Microbe Interactions*, Poole, R.K. and Gadd, G.M, Eds., Oxford: IRL Press, 1989, pp. 85–98.

Burov, B.V., Nurgaliev, D.K., and Yasonov, P.G., *Paleomagnitnyi analiz* (Paleomagnetic analysis), Kazan: KGU, 1986.

Day, R., Fuller, M., and Schmidt, V.A., Hysteresis properties of titanomagnetites: grain-size and compositional dependence, *Phys. Earth Planet. Inter.*, 1977, vol. 13, pp. 260–267.

Dunlop, D.J. and Özdemir, Ö., *Rock Magnetism: Fundamentals and Frontiers*, Cambridge: Cambridge Univ. Press, 1997.

Egli, R., Analysis of the field dependence of remanent magnetization curves, *J. Geophys. Res. B: Solid Earth*, 2003, vol. 108, no. 2, pp. EPM 4-1– EPM 4-25.

Egli, R., Characterization of individual rock magnetic components by analysis of remanence curves: 1. Unmixing natural sediments, *Stud. Geophys. Geod.*, 2004a, vol. 48, no. 2, pp. 391–446.

Egli, R., Characterization of individual rock magnetic components by analysis of remanence curves: 2. Fundamental properties of coercivity distributions, *Phys. Chem. Earth*, 2004b, vol. 29, nos. 13–14, pp. 851–867.

Egli, R., Characterization of individual rock magnetic components by analysis of remanence curves: 3. Bacterial magnetite and natural processes in lakes, *Phys. Chem. Earth*, 2004c, vol. 29, nos. 13–14, pp. 869–884.

Evans, M.E. and Heller, F., *Environmental Magnetism. Principles and Applications of Enviromagnetics*, San Diego: Academic, 2003.

Fedotov, A.P., Chebykina, E.P., Semenov, M.Yu., Vorobyovaa, S.S., et al., Changes in the volume and salinity of Lake Khubsugul (Mongolia) in response to global climate changes in the Upper Pleistocene and the Holocene, *Palaeogeogr., Palaeoclimatol., Palaeoecol,*, 2004, vol. 209, pp. 245–257.

Garming, J.F.L., Bleil, U., and Riedinger, N., Alteration of magnetic mineralogy at the sulphate-methane transition: analysis of sediments from the Argentine continental slope, *Phys. Earth Planet. Inter.*, 2005, vol. 151, pp. 290–308.

Grygar, T., Dekkers, M.J., Bezdicka, P., Schneeweiss, O., Dedecek, J., and Kruiver, P.P., Iron oxide mineralogy in Late Miocene red beds from La Gloria, Spain: rock-magnetic, voltammetric and Vis spectroscopy analyses, *Catena*, 2003, vol. 53, pp. 115–132.

Heslop, D., Dekkers, M.J., Kruiver, P.P., and Oorschot, I.H.M., Analysis of isothermal remanent magnetization acquisition curves using the expectation-maximization algorithm, *Geophys. J. Int.*, 2002, vol. 148, pp. 58–64.

Heslop, D., Witt, A., Kleiner, T., and Fabian, K., The role of magnetostatic interactions in sediment suspensions, *Geophys. J. Int.*, 2006, vol. 165, pp. 775–785.

Heslop, D. and Dillon, M., Unmixing magnetic remanence curves without a priori knowledge, *Geophys. J. Int.*, 2007, vol. 170, no. 2, pp. 556–566.

Heslop, D. and Roberts, A.P., A method for unmixing magnetic hysteresis loops, *J. Geophys. Res.: Solid Earth*, 2012, vol. 117, no. B3. doi 10.1029/2011JB008787

Heywood, B.R., Bazylinski, D.A., Garrett-Reed, A., Mann, S., and Frankel, R.B., Controlled biosynthesis of greigite (Fe_3S_4) in magnetotactic bacteria, *Natur-wissen-* 1 *schaften*, 1990, vol. 77, pp. 536–538.

Ivanov, V.A., Khaburzaniya, I.A., and Sholpo, L.E., Using the Preisach diagram for diagnosing single- and multidomain grains in the rock samples, *Izv. Akad. Nauk SSSR, Fiz. Zemli*, 1981, no. 1, pp. 55–65.

Kochegura, V.V., On the analysis of the curve of normal remanent magnetization, in *Nastoyashchee i proshloe magnitnogo polya Zemli* (The Present and the Past of the Earth's Magnetic Field), 1965, pp. 154–157.

Kruiver, P.P., Dekkers, M.J., and Heslop, D., Quantification of magnetic coercivity components by the analysis of acquisition curves of isothermal remanent magnetization, *Earth Planet. Sci. Lett.*, 2001, vol. 189, pp. 269–276.

Kruiver, P.P. and Passier, H.F., Coercivity analysis of magnetic phases in sapropel S1 related to variations in redox conditions, including an investigation of the S ratio, *Geochem. Geophys. Geosyst.*, 2001, vol. 2, no. 12. doi 10.1029/2001GC000181

Mann, S., Frankel, R.B., and Blakemore, R.P., Structure, morphology, and crystal growth of bacterial magnetite, *Nature (London)*, 1984, vol. 310, pp. 405–407.

Moreau, F., Gibert, D., Holschneider, M., and Saracco, G., Identification of sources of potential fields with the continuous wavelet transform: basic theory, *J. Geophys. Res.*, 1999, vol. 104, no. B3, pp. 5003–5013.

Nourgaliev, D.K., Yasonov, P.G., Kosareva, L.R., Kazanskii, A.Yu., and Fedotov, A.P., The origin of magnetic minerals in the Lake Khubsugul sediments (Mongolia), *Rus. J. Earth Sci.*, 2005, vol. 7, no. 3, pp. 1–6.

van Oorschot, I.H.M., Dekkers, M.J., and Havlicek, P., Selective dissolution of magnetic iron oxides with the acid-

ammonium-oxalate/ferrousiron extraction technique: II. Natural loess and palaeosol samples, *Geophys. J. Int.*, 2002, vol. 149, pp. 106−117.

Pechersky, D.M., Grachev, A.F., Nourgaliev, D.K., Tselmovich, V.A., and Sharonova, Z.V., Magnetolithologic and magnetomineralogical characteristics of deposits at the Mesozoic/Cenozoic boundary: Gams section (Austria), *Rus. J. Earth Sci.*, 2006, vol. 8, no. 3, ES3001.

Robertson, D.J. and France, D.E., Discrimination of remanence-carrying minerals in mixtures, using isothermal remanent magnetisation acquisition curves, *Phys. Earth Planet. Inter.*, 1994, vol. 82, pp. 223−234.

Shcherbakov, V.P., Lamash, B.E., and Shcherbakova, V.V., *Fizika magnetizma gornykh porod* (Physics of Rock Magnetism), Moscow: IFZ AN SSSR, 1991.

Sholpo, L.E., *Ispol'zovanie magnetizma gornykh porod dlya resheniya geologicheskikh zadach* (Using the Rock Magnetism for Solving Geological Tasks), Leningrad: Nedra, 1977.

Spassov, S., Heller, F., Kretzschmar, R., Evans, M.E., Yue, L.P., and Nourgaliev, D.K., Detrital and pedogenic magnetic mineral phases in the loess/paleosol sequence at Lingtai (Central Chinese Loess Plateau), *Phys. Earth Planet. Inter.*, 2003, vol. 140, pp. 255−275.

Spassov, S., Egli, R., Heller, F., Nourgaliev, D.K., and Hannam, J., Magnetic quantification of urban pollution sources in atmospheric particulate matter, *Geophys. J. Int.*, 2004, no. 159, pp. 555−564.

Stockhausen, H., Some new aspects for the modelling of isothermal remanent magnetization acquisition curves by cumulative log Gaussian functions, *Geophys. Rev. Lett.*, 1998, vol. 25, pp. 2217−2220.

Thompson, R., Modelling magnetization data using SIMPLEX, *Phys. Earth Planet. Inter.*, 1986, vol. 42, pp. 113−127.

Tundisi, J.G. and Matsumura-Tundisi, T., *Limnology*, Leiden: CRC Press/Balkema, 2011.

Utemov, E.V. and Nurgaliev, D.K., Natural wavelet transformations of gravity data: theory and applications, *Izv., Phys. Solid Earth*, 2005, vol. 41, no. 4, pp. 333−344.

Wetzel, R.G., *Limnology: Lake and River Ecosystems, 3rd ed.*, San Diego: Academic, 2001.

Translated by M. Nazarenko

SPELL: 1. greigite, 2. thermomagnetic, 3. biogenic